



## Preparation of an activated carbon involving magnetic properties

Bahia Baaziz<sup>a,b</sup>, Madani Drouiche<sup>a</sup>, Nadjib Drouiche<sup>a,c,\*</sup>, Sarah Nour<sup>a</sup>, Hakim Lounici<sup>a,d,\*</sup>

<sup>a</sup>URIE, Ecole Nationale Polytechnique d'Alger, BP 182, 10 Avenue Pasteur El Harrach 16200, El Harrach, Alger, Algeria, emails: [mdrouiche@yahoo.fr](mailto:mdrouiche@yahoo.fr) (M. Drouiche), [nadjibdrouiche@yahoo.fr](mailto:nadjibdrouiche@yahoo.fr) (N. Drouiche), [chemin.deux@gmail.com](mailto:chemin.deux@gmail.com) (S. Nour), [Hakim.lounici@yahoo.fr](mailto:Hakim.lounici@yahoo.fr) (H. Lounici)

<sup>b</sup>Department of Environmental Engineering, Université UMMTO Tizi Ouzou, Campus Bastos, Tizi Ouzou, Algeria

<sup>c</sup>Department of Environmental Engineering, Centre de Recherche en Technologie des Semi-conducteurs pour l'Energétique (CRTSE), 2, Bd Frantz Fanon BP140, Alger—7 Merveilles, 16027, Algeria

<sup>d</sup>Department of Environmental Engineering, Université de Bouira, Pôle technologique, Bouira, Algeria

Received 26 December 2015; Accepted 13 February 2016

### ABSTRACT

Magnetic activated carbon composite (MAC) was successfully prepared from olive residues and hematite (Fe<sub>2</sub>O<sub>3</sub>/AC). MAC was prepared based on a wet impregnation method followed by carbonization, under different operating conditions. Specifically, two different MACs were prepared by altering the temperature ramp rate during the carbonization procedure (5 and 20 min/°C), designated here as MAC<sup>5</sup> and MAC<sup>20</sup>, respectively. The increased magnetic capacity of the two MACs (as evidenced by the measured permanent magnetism of 30 mT), allowed their easy separation by utilizing a simple magnetic separation technology. The efficient impregnation of the iron oxide on the two MACs was confirmed by Fourier transform infrared spectroscopy (FT-IR), while scanning electron microscopy (SEM) was used to characterize the morphology of the composites. FT-IR measurements showed the appearance of new peaks, between 500 and 700 cm<sup>-1</sup> which is evidence of the effective binding of iron onto AC (C/Fe). The SEM images offered an insight to the size and the distribution of the pores on the MAC, which appeared to be much better than the pure AC. The magnetic separation was examined through mass balances, before and after applying the magnetic field. The results showed that the magnetic efficiency of MAC<sup>5</sup> is higher compared to that of MAC<sup>20</sup>. The magnetic properties of the produced MAC pave the way for their utilization in magnetic separation methods.

*Keywords:* Hematite; Coil; Magnetic activated carbon; Characterization; Magnetic field

### 1. Introduction

Water is the single most important nutrient of life and is essential for the human body functions. Unfortunately, access to safe drinking water is not available all over the world. Moreover, there is an increase in

water pollution in all forms what led to new materials technologies for wastewater treatment.

Various adsorbent have been used, mainly residues of olive activated carbon, which is highly used since it is considered a very effective adsorbent [1–10] for the purification of contained environments and also contributes to minimizing the solid wastes. Nevertheless, its application fields are restricted due to its high cost.

\*Corresponding authors.

Therefore, the use of low-cost wastes and agriculture by-products to produce activated carbon has been shown to provide economical solution to this problem [11,12].

However, the use of no magnetic activated carbon involves certain problems since it is very difficult to recover it from wastewater. Consequently, modified activated carbon on its core structure is developed, especially on magnetic properties bringing new approaches related to the separation of the magnetic activated ferromagnetism carbon from waste water by applying an external magnetic field. Therefore, it is easy for recovery and reuse.

Magnetism represents an interesting phenomenon that has attracted human attention for many years. Nowadays, magnetism is the basic principal of many devices, procedures, and technologies. However, this phenomenon has also found really important applications only relatively recently in various areas of biosciences and biotechnologies [13]. Permanent magnets have persistent magnetic fields caused by ferromagnetism, which is the strongest and most familiar type of magnetism [14]. The  $\text{Fe}_2\text{O}_3$  actually called iron (III) oxide, better known as hematite or rust which has ferromagnetic properties and can be used in magnetic separation under magnetic field allowing a better control on the magnetic properties. In addition iron (Fe), cobalt (Co), nickels (Ni) and manganese (Mn) have very large magnetic permeability [15]. There different magnetic field sources such as; permanent magnet, solenoid, etc. which provide a simple means to generate a strong magnetic field. When a current passes through the solenoid, it creates a nearly uniform magnetic field inside.

Recently, magnetic activated carbon has attracted an increasing interest, due to their unique magnetic properties as well as much potential application in magnetic data storage devices [16] and water treatment [17]. Nevertheless, very few data have been published on the magnetic and conducting properties of composites with shell structure, such as magnetic activated carbon with ferromagnetic particles. Such materials have special interest because of new and often usual electromagnetic properties [18].

The aim of the present work is to prepare a new material based on hematite-supported activated carbon under suitable magnetic properties in batch mode operation. The permanent magnet was used only for the ease phase separation.

## 2. Materials and methods

Hematite ( $\text{Fe}_2\text{O}_3$ ) and hydrogen chloride (HCl 37%) were purchased from Merck (Germany).

Carbonization was used in the conventional furnace type (PROLABO, VOLCA MC18). Activation carbon was used in tubular furnace type (Carbolite, eurotherm 2416 CG). An electric generator type the magnetic field  $B$  inside the coil was measured by a Teslameter (type (DF390) connected to an electric generator (MCP lab electronics, model: M10-TP 3003L).

The magnetic field  $B$  inside the coil was measured by a Tesla meter connected to an electric generator. A rectangular permanent magnet (30 mT) is chosen as the magnetic field source for the phase separation. The value of the magnetic field is measured (in Milli-Tesla, mT) inside the coil. However, this effect disappears when the applied field is removed.

Infrared spectroscopy was used to obtain information about the chemical structure and functional groups of the carbon, prepared activated carbon and the magnetic activated carbon. The FT-IR spectra of each sample were scanned by placing KBr pellets in the Fourier transform spectrophotometer SHIMATZU 8,400. The KBr pellets were prepared by mixing 0.2 g of each sample with KBr, grounding it in an agate mortar and then shaping it into pellets under hydraulic pressure.

*Morphological* structures were studied with scanning electron microscopy (SEM) (Philips ESEMXL30) to show the morphology of the surface of the sample to any change observed.

### 2.1. Preparation of the magnetic activated carbon, activated carbon and carbon

First, an amount of residues olive precursor (RO) (10 g) was impregnated into a 40-ml suspension of hematite  $\text{Fe}_2\text{O}_3$  (1.25 mmol/g), used as magnetic precursor. HCl (12 N) was used as carbon modifying agent at room temperature during 24 h. Then, the impregnated activated carbons were filtrated and further dried in an oven at 105°C. Finally, they were treated at 800°C with a heating rate 5 and 20°C/min during 1 h in the tubular furnace in the presence of water vapor. The samples were washed with cold distilled water and dried in an oven at 105°C.

The obtained carbons are denoted as  $\text{MAC}^5$  and  $\text{MAC}^{20}$ , respectively. The magnetic activated carbon was disposed in the artisanal coil under an applied magnetic field of 6 mT. The same procedure using activated carbon, AC, as precursor was carried out. The synthesis of a blank  $\text{AC}^5$  and  $\text{AC}^{20}$  sample followed the same procedure except the impregnation solution. The carbon was carbonized at 500°C during 10 min in the conventional furnace. Then, the carbon was washed with distilled water and dried in an oven at 105°C.

Samples were characterized and results are listed in Table 1. It should be noted that the real density and the apparent density are close enough for both active carbon and magnetic activated carbon. Measurements indicated also, that the micro pore volume of activated carbon AC were higher than Magnetic activated carbon MAC. No significant decrease in the porosity of activated carbon AC was caused by the presence of the hematite.

The general schematic diagram for the preparation of magnetic activated carbon was given in Fig. 1.

### 2.1.1. Magnetic field of a solenoid

One common and important magnetic field source is the solenoid; mostly used to provide the magnetic field, within the coil; a strong magnetic field arises whenever current is run through the wire. The direction of the magnetic field depends on the direction of current. Outside the coil, the magnetic field is small [19].

In order to increase its magnetic field, an artisanal coil was prepared at the laboratory scale. The copper wire was wrapped tightly around a cylinder of 30 mm providing a magnetic field up to 11 mT. Table 2 gives the most common parameters of artisanal and commercial coil. This artisanal coil allowed us to smoothly vary the magnetic field  $B$  and fixe it at any given point  $B$ .

A solenoid is a long coil of wire wrapped in many turns. The magnetic field within a solenoid depends upon the current and density of turns Ampere’s law allows us to calculate the strength of the magnetic field. Inside the coil, the field lines are always oriented from the South Pole to the North Pole to form closed Loops. The direction of the field is parallel to the axis of the solenoid. There is no field outside the solenoid.

The magnetic field in the center of the coil is written as:

$$B = \frac{\mu_0 NI}{l} \tag{1}$$

where  $B$ : the magnetic field inside the coil, in Tesla,  $N$ : the number of turns of wire per meter,  $I$ : the current through wire, in amperes,  $l$ : the length of the coil, and  $\mu_0$ : the permeability constant (Fig. 2).

To give more details about the behavior of both coils, standard curves were obtained (Fig. 3). The value of the field generated by a coil is proportional to the intensity of the current passing through it (i.e. graph  $B = f(I)$  is a straight line passing through the origin).

### 2.1.2. Magnetic separation

The evolution of the magnetic separation rate (MSR) for the magnetic activated carbon versus induction time for both precursors resides olive and activated carbon were studied (Fig. 4). Results show that a total of magnetic separation, i.e. 100% of MAC<sup>5</sup>, taken as olive resides precursors took place. However, only 42.1% was observed for the activated carbon precursor. It may be explained that the hydrogen chloride used as carbon modifying agent play a great influence on the surface area on the raw material than the calcined form. Consequently, residues olives magnetic activated carbon was shown to be a promising and attracting new adsorbent.

The MSR is calculated by the following formula:

$$MSR = \frac{\text{Final mass of MAC}}{\text{Initial mass of MAC}} \tag{2}$$

where MSR: magnetic separation rate (%); Final mass of MAC: mass of the remaining magnetic activated carbon after permanent magnet application; and Initial mass of MAC: total mass of the magnetic activated carbon.

Fig. 5 shows a bar histogram of the magnetic separation rate (%) (MSR) with all parameters Viz. [HCl], hematite mass, magnetic field; it can be noted that while [HCl] = 12 N and the mass of hematite is taken 1.25 mmol/g and the applied magnetic field is maintained at 6 mT, the optimum percentage of MSR is observed.

Table 1  
Characteristics of the magnetic activated carbon, activated carbon, and carbon

	Dr (g/cm <sup>3</sup> )	Da (g/cm <sup>3</sup> )	Porosity	VPT (cm <sup>3</sup> )	pH	I <sub>2</sub> (mg/g)	Conductivity (μS)	Humidity (%)
MAC <sup>20</sup>	596.97	356.99	0.402	0.804	7.59	933.45	15	7.22
MAC <sup>5</sup>	649.35	421.42	0.351	0.702	8.73	876.30	19.5	7.02
AC <sup>20</sup>	668.20	389.60	0.417	0.833	7.28	717.55	15.4	8.47
AC <sup>5</sup>	694.76	441.30	0.365	0.730	7.89	476.25	17.6	8.81

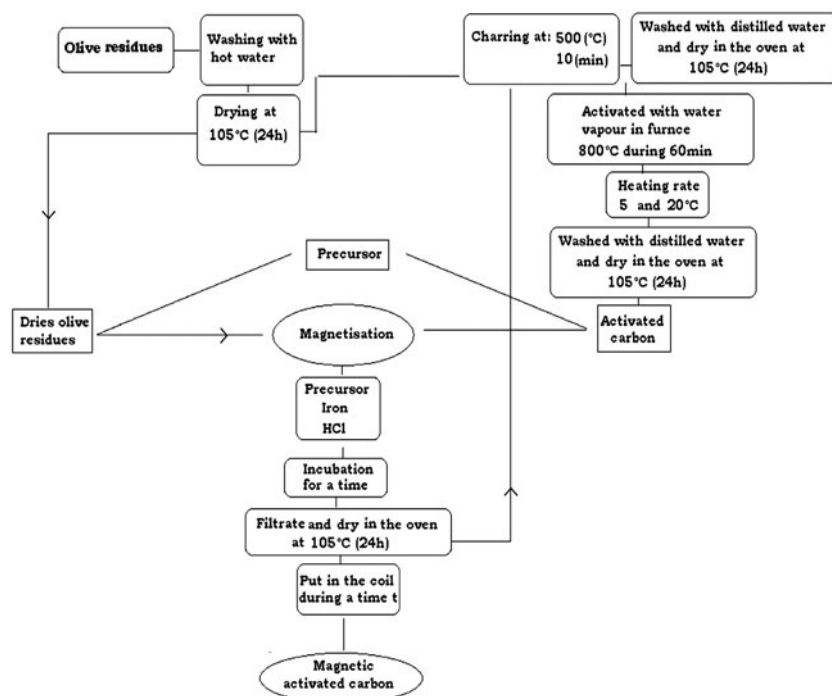


Fig. 1. Schematic diagram of the preparation of magnetic activated carbon.

Table 2

Characteristics of both coils used in the magnetic induction

Coil	Commercial (a)	Artisanal (b)
Source	Phywe (1100100)	Laboratory (URIE)
Number of turns of wire	485	600
Length (cm)	75	10
Diameter (mm)	79	30
Resistance $R$ ( $\Omega$ )	0.3	0.6
Diameter of the wire (mm)	–	0.8

### 3. Results and discussion

#### 3.1. Effect of the iron solution

The effects of the iron oxide solutions and iron salt solutions as impregnated agent versus induction time for the preparation of the magnetic activated carbon were studied (Fig. 6). It is evident that the values of the  $\text{Fe}_2\text{O}_3$  were far greater than  $\text{FeO}$  and the ferrous and ferric salt solution which their curves are grouped closely together with the MSR takes quite small values. It may be due to the oxidation for the ferrous and ferric solution making them least effective.

#### 3.2. Effect of the distance

The following graph shows the magnetic separation rate (%) versus the distance towards the magnetic activated carbon MCA<sup>5</sup>. The curves are obtained at three different permanent applied fields  $B$ : 48 mT (upper curve), 26 mT (middle curve) and 15 mT (lower curve) (Fig. 7). The layout of the curves (middle and lower curve are the same as the upper one). However, the gap between curves may be due to the magnetic field power. It is evident that permanent magnetic field (i.e.  $B = 48$  mT) has more attractive power than the others consequently; has more magnetic separation rate.

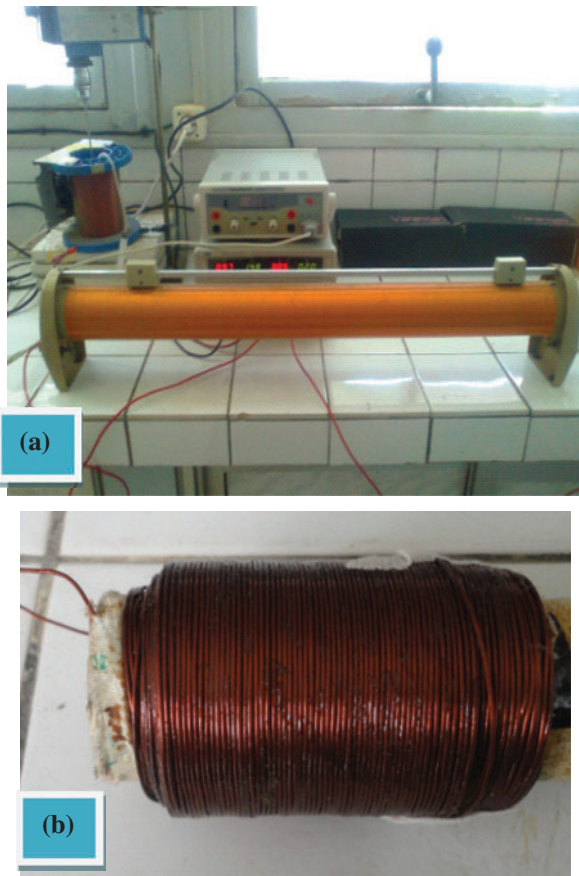


Fig. 2. Commercial coil (a) and artisanal coil (b) used in this work.

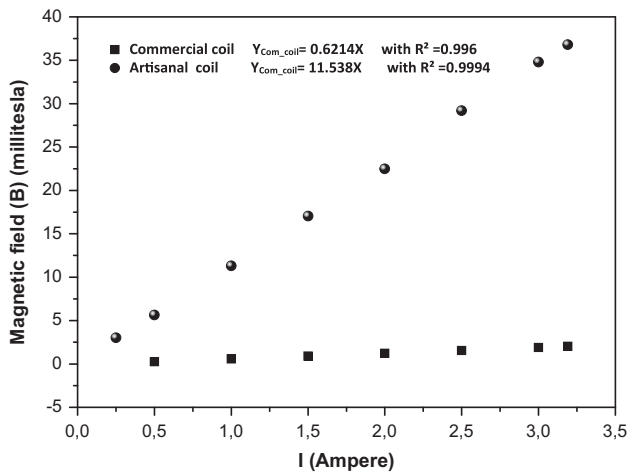


Fig. 3. Standard curves of both coils:  $\blacksquare$ —commercial coil,  $V = 1.9$  volt;  $\bullet$ —artisanal coil  $V = 11.3$  volt.

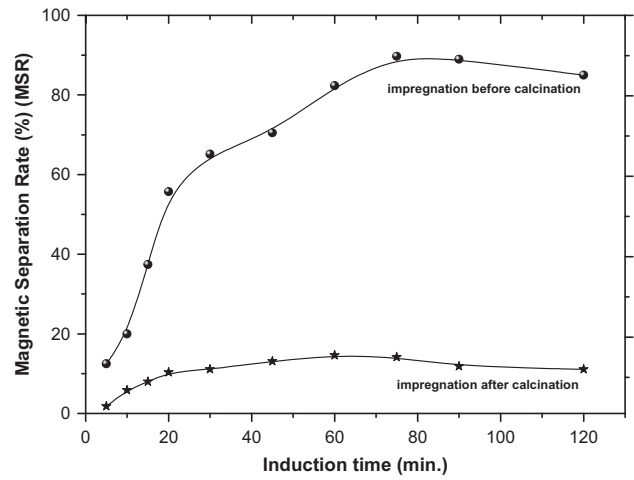


Fig. 4. Magnetic separation rate (%) (MSR) vs. induction time (Viz.  $[HCl] = 12$  N, iron mass =  $1.125$  mmol/g, Induction field  $B = 6$  mT ).  $\star$ —impregnation after calcination;  $\bullet$ —impregnation before calcination.

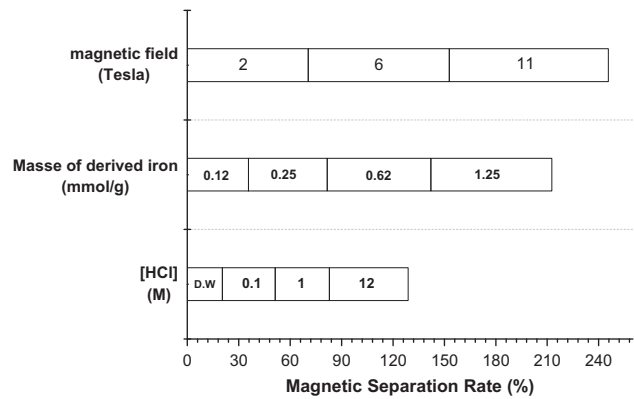


Fig. 5. Bar histogram of the magnetic separation rate (%) (MSR) with all parameters (Viz.  $[HCl]$ , hematite mass, magnetic field).

### 3.3. Adsorption kinetic and equilibrium isotherm

Adsorption kinetic and equilibrium isotherm of the magnetic activated carbon  $MAC^5$  using pseudo-first and second-order kinetic equations, the intra-particle diffusion model, as well as Freundlich, Langmuir and Temkin models were studied. The equilibrium data of the magnetic activated carbon was found to best fit to the Langmuir model for the magnetic activated carbon at  $800^\circ C$ ,  $5^\circ C/min$ . Moreover, the results showed that the pseudo-second-order with reactant MB was appropriate kinetic model.

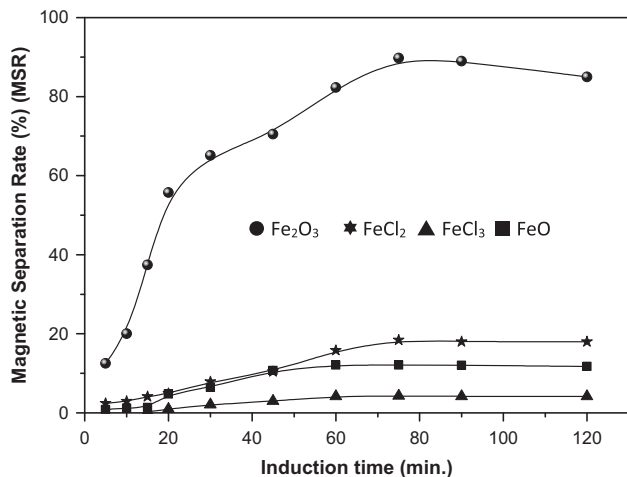


Fig. 6. The effects of the iron oxide and salt solutions vs. induction time (Viz.  $[HCl] = 12\text{ N}$ , iron mass = 1.125 mmol/g, Induction field  $B = 6\text{ mT}$ ).

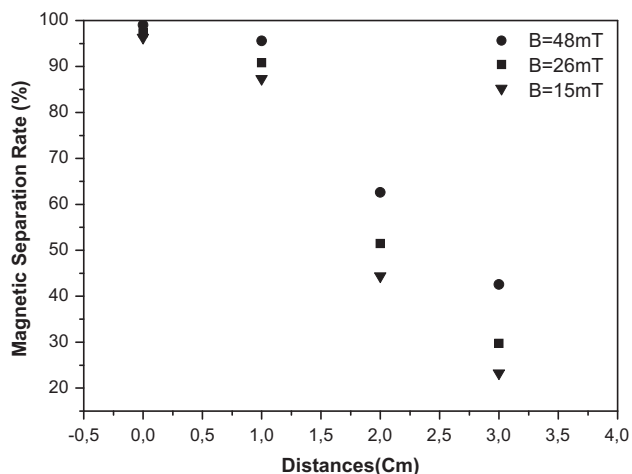


Fig. 7. The effect of the permanent magnetic field vs. the distance for the  $MCA^5$  (Viz.  $800^\circ\text{C}$ , 5 min/ $^\circ\text{C}$ , 1 h,  $[HCl] = 12\text{ N}$ ).

### 3.4. FT-IR studies

The FTIR spectrum of the magnetic activated carbon  $MAC^5$ , activated carbon  $AC^5$  carried out at optimum operating condition and the carbon C (Fig. 8) showed the characteristic bands and the comparison of these three samples.

The band located at  $3,630\text{ cm}^{-1}$  (spectrum C) correspond to the bending vibration of the free alcohol (fine bound) H–OH–H. It disappears after activation.

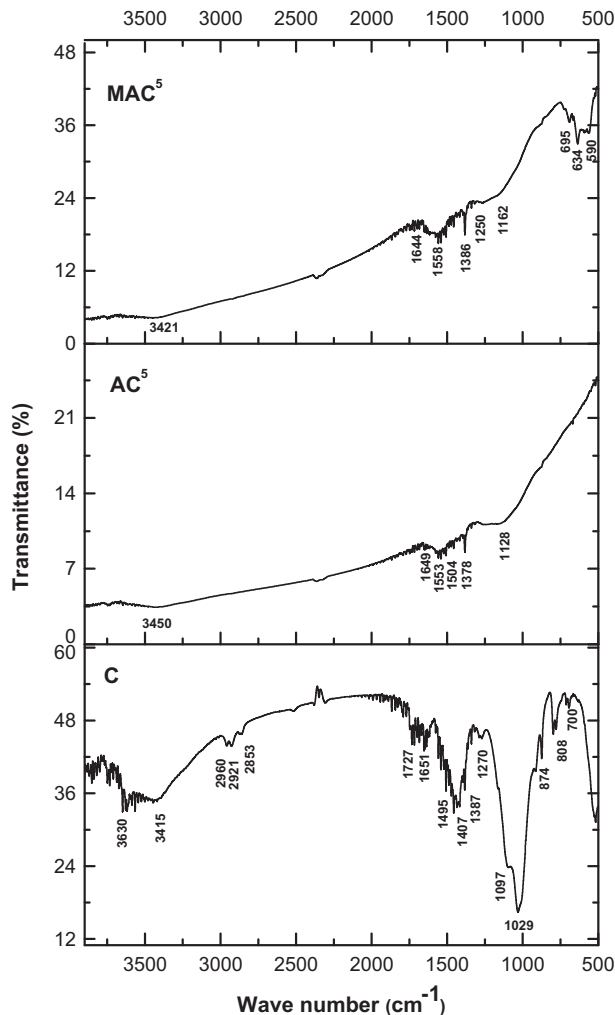


Fig. 8. FTIR spectra of the magnetic activated carbon ( $MAC^5$ ) (i.e.  $[HCl] = 12\text{ N}$ , iron mass = 1.125 mmol/g, induction field  $B = 6\text{ mT}$ ), activated carbon ( $AC^5$ ) (i.e. temperature of activation =  $800^\circ\text{C}$  during 60 min), carbon (C) (i.e. temperature of carbonization =  $500^\circ\text{C}$ , during 10 min). SEM Studies.

The band located at 3,415, 3,450 and 3,421 for all spectra correspond to the fine bound of free alcohol (of water) H–OH–H [20] and remained unaffected even after magnetization the sample. However, a dramatic decrease in intensity of the bands of the carbon C compared to  $MAC^5$  and  $AC^5$  due to the physically activation temperature at  $800^\circ\text{C}$  which carbonized all organic matter.

A disappearance of bands ( $2,960\text{--}2,921\text{--}2,853\text{ cm}^{-1}$ ) on the  $AC^5$  and  $MAC^5$  spectrum that indicate the C–H vibrations in methyl and methylene groups (on spectrum C); this disappearance is due to the high-activated temperature ( $800^\circ\text{C}$ ) and the duration of the activation (60 min).

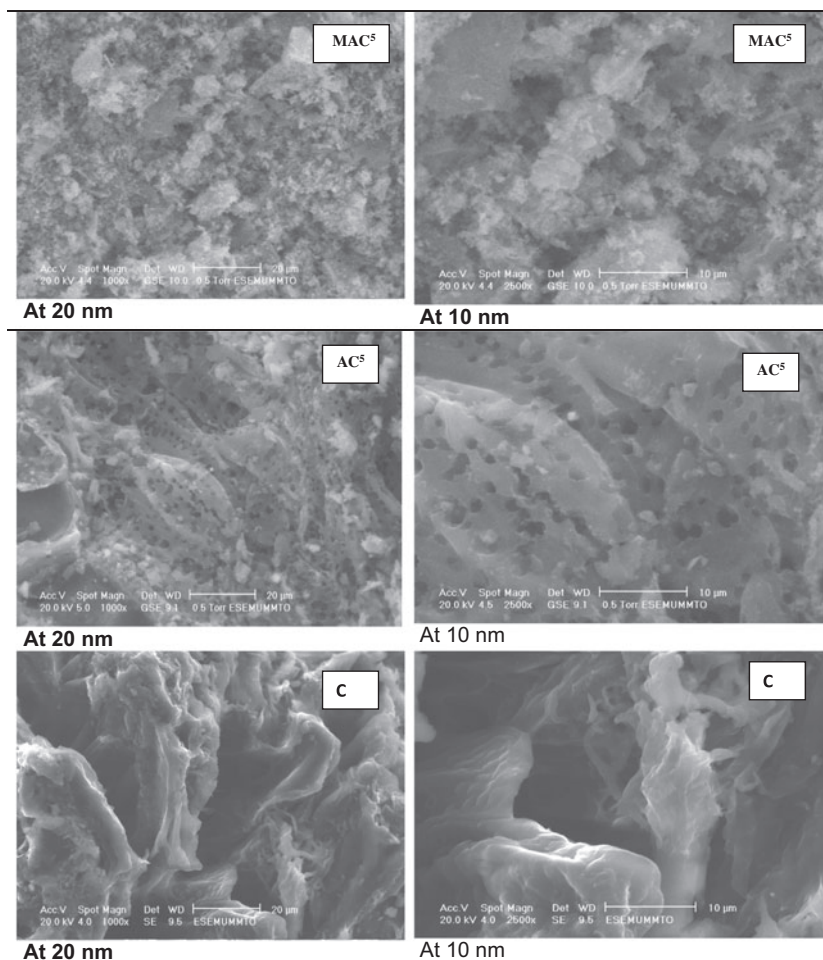


Fig. 9. SEM micrographs of the magnetic activated carbon (MAC<sup>5</sup>) (i.e. [HCl] = 12 N, iron mass = 1.125 mmol/g, Induction field  $B = 6$  mT), activated carbon (AC<sup>5</sup>) (i.e. temperature of activation = 800°C during 60 min), carbon (C) (i.e. temperature of carbonization = 500°C, during 10 min).

The band located at  $1,727\text{ cm}^{-1}$  is assigned to carbonyl C=O groups on the C spectrum disappear on the spectra (AC<sup>5</sup> and MAC<sup>5</sup>). It shifts to 1,649 and 1,644 in spectrum AC<sup>5</sup> and MAC<sup>5</sup>, respectively.

The olefinic C=C vibrations cause the emergence of the band at about  $1,651\text{ cm}^{-1}$  in C, while the skeletal C=C vibrations in aromatic rings cause a band at  $1,553\text{ cm}^{-1}$  in AC<sup>5</sup> and at  $1,558\text{ cm}^{-1}$  in MAC<sup>5</sup> [20].

The vibration at  $1,495\text{ cm}^{-1}$  is assigned to the bands CH<sub>3</sub> and CH<sub>2</sub>. The band  $1,407\text{ cm}^{-1}$  is assigned to  $\nu(\text{C}-\text{O})$  vibrations in carboxylate groups (Spectrum C). It shifts to 1,128 and 1,162 in spectrum AC<sup>5</sup> and MAC<sup>5</sup>, respectively, may be due to the high carbonization.

At 1,378, 1,378, and  $1,386\text{ cm}^{-1}$  for the three spectra is attributed to the OH carboxylic acids –OH. The band at  $1,270\text{ cm}^{-1}$  may be attributed to ester

(R–CO–O–R') or ethers R–O–R' or phenol groups this band disappears in the AC<sup>5</sup> and MAC<sup>5</sup>.

The intense band at  $1,029\text{ cm}^{-1}$  can be assigned to alcohol groups (R–OH). This band disappears in the AC<sup>5</sup> and MAC<sup>5</sup>.

The intense band at  $1,029\text{ cm}^{-1}$  can be assigned to alcohol groups (R–OH). This band disappears in the AC<sup>5</sup> and MAC<sup>5</sup>. The intense band at  $1,029\text{ cm}^{-1}$  can be assigned to alcohol groups (R–OH). This band disappears in the AC<sup>5</sup> and MAC<sup>5</sup>.

In addition, the bands  $1,634\text{ cm}^{-1}$  were ascribed to the H–O–H bending vibration of the absorbed water [20]. Nevertheless, its remaining waves number at 1,600–1,533 and 1,378 corresponding to ionize carboxylic acid.

On the AC<sup>5</sup> spectra show that the temperature of activation 800°C has a great influence on the disappearance of the bands 874, 808, and  $700\text{ cm}^{-1}$

correspond to the C–H out of plane bending in benzene derivative vibrations, the additional –OH and C–H in benzene. On the other hand, there is no difference between MAC<sup>5</sup> and AC<sup>5</sup> only in the range [900–500 cm<sup>-1</sup>] indicating the attachment of the iron on the structure of the carbon (F–O).

The morphology of the all samples was investigated by SEM and is shown in Fig. 9. The spectrum C had a porous surface. After activation with air AC<sup>5</sup>, a continuous over-layer is produced on the blank carbon. The effect of the hematite addition on the AC<sup>5</sup> surface formed new pores on MAC<sup>5</sup> that will improve or maintain the high surface area and porosity of activated carbon [20].

#### 4. Conclusion

The magnetic activated carbon was prepared from olive residues taken from Kabylia region under suitable conditions in batch mode ([hematite = 1.25 g/mol], [HCl] = 12 N, *t* = 1 h) Viz. (MAC<sup>5</sup>, MAC<sup>20</sup>). Activated carbon (AC<sup>5</sup>, AC<sup>20</sup>), as well as carbon C were also prepared at (500°C, 5 and 20 min/°C, 10 min) Viz. and (Viz. 500°C, 10 min), respectively, and being impregnated with hematite commonly known as an iron(III) oxide in powder form Fe<sub>2</sub>O<sub>3</sub>.

IR and SEM results for the magnetic activated carbon show that have successfully formed. The separation magnetic rate data suggested a total of magnetic separation rate, i.e. 100% of MAC<sup>5</sup> taken as olive residues precursors, however, only 42.1% is observed for the activated carbon precursor.

Magnetic separation rate is strongly influenced by the magnetic field that will vary with its attraction power. Micropore volume of activated carbon AC was higher than magnetic activated carbon MAC. No significant decrease in the porosity of activated carbon AC was caused by the presence of the hematite.

Magnetic activated carbon MAC can be used to remove hazardous material in wastewater treatment systems since they have high adsorption capacities and can be separated easily from the medium by application of a permanent magnetic field.

#### Acknowledgment

The authors are grateful to the Mouloud Mammeri University of Tizi Ouzou (UMMTO) for IR, SEM spectra.

#### References

- [1] R. Baccar, J. Bouzid, M. Feki, A. Montiel, Preparation of activated carbon from Tunisian olive-waste cakes and its application for adsorption of heavy metal ions, *J. Hazard. Mater.* 162 (2009) 1522–1529.
- [2] A.A.M. Daifullah, S.M. Yakout, S.A. Elreefy, Adsorption of fluoride in aqueous solutions using KMnO<sub>4</sub>-modified activated carbon derived from steam pyrolysis of rice straw, *J. Hazard. Mater.* 147 (2007) 633–643.
- [3] H. Lounici, F. Aiouche, D. Belhocine, M. Drouiche, A. Pauss, Mechanism of phenol adsorption onto electro-activated carbon granules, *Water Res.* 38 (2004) 218–224.
- [4] O. Kitous, H. Hamadou, H. Lounici, N. Drouiche, N. Mameri, Metribuzin removal with electro-activated granular carbon, *Chem. Eng. Process.* 55 (2012) 20–23.
- [5] O. Kitous, N. Abdi, H. Lounici, H. Grib, N. Drouiche, E.H. Benyoussef, N. Mameri, Modeling of the adsorption of metribuzin pesticide onto electro-activated granular carbon, *Desalin. Water Treat.* 57 (2016) 1865–1873.
- [6] O. Yahiaoui, H. Lounici, N. Abdi, N. Drouiche, N. Ghaffour, A. Pauss, N. Mameri, Treatment of olive mill wastewater by the combination of ultrafiltration and bipolar electrochemical reactor processes, *Chem. Eng. Process.* 50 (2011) 37–41.
- [7] N. Drouiche, H. Grib, N. Abdi, H. Lounici, A. Pauss, N. Mameri, Electrodialysis with bipolar membrane for regeneration of a spent activated carbon, *J. Hazard. Mater.* 170 (2009) 197–202.
- [8] N. Drouiche, H. Mahmoudi, N. Mameri, H. Lounici, N. Ghaffour, Utilization of electro-dialysis for the regeneration of granular activated carbon packed in beds saturated with H<sub>2</sub>S, *Desalination* 200 (2006) 629–631.
- [9] M. Pirsahab, Z. Rezai, A.M. Mansouri, A. Rastegar, A. Alahabadi, A. Rahmani Sani, K. Sharafi, Preparation of the activated carbon from India shrub wood and their application for methylene blue removal: Modeling and optimization, *Desalin. Water Treat.* 57(13) (2016) 5888–5902.
- [10] M. Caccin, M. Giorgi, F. Giacobbo, M. Da Ros, L. Besozzin, M. Mariani, Removal of lead (II) from aqueous solutions by adsorption onto activated carbon prepared from coconut shell, *Desalin. Water Treat.* 57 (10) (2016) 4557–4575.
- [11] O. Ioannidou, A. Zabaniotou, Agricultural residues as precursors for activated carbon production—A review, *Renewable Sustainable Energy Rev.* 11 (2007) 1966–2005.
- [12] G. Cimino, R.M. Cappello, C. Caristi, G. Toscano, Characterization of carbons from olive cake by sorption of wastewater pollutants, *Chemosphere* 61 (2005) 947–955.
- [13] I. Safari, M. Safarikova, Magnetic nano- and microparticles in biotechnology, *Chem. Papers* 63 (2009) 497–505.
- [14] U. Blaha, B. Sapkota, E. Appel, H. Stanjek, W. Rosler, Micro-scale grain-size analysis and magnetic properties of coal-fired power plant fly ash and its relevance for environmental magnetic pollution studies, *Atmospheric Environ.* 42 (2008) 8359–8370.

- [15] C.H. Chia, S.D. Joseph, A. Rawal, R. Linser, J.M. Hook, P. Munroe, Microstructural characterization of white charcoal, *J. Anal. Appl. Pyrolysis* 109 (2014) 215–221.
- [16] Q. Liu, Z.G. Chen, B. Liu, W. Ren, F. Li, H. Cong, H.M. Cheng, Synthesis of different magnetic carbon nanostructures by the pyrolysis of ferrocene at different sublimation temperatures, *Carbon* 46 (2008) 1892–1902.
- [17] R.D. Ambashta, M. Sillanpää, Water purification using magnetic assistance: A review, *J. Hazard. Mater.* 180 (2010) 38–49.
- [18] V. Pode, E. Popovici, R. Pode, V. Georgescu, Magnetic properties of an adsorbent based on modified natural zeolite, *Revue roumaine de chimie* 52(2007) (2007) 983–989.
- [19] L. Lerner, Magnetic field of a finite solenoid with a linear permeable core, *Am. J. Phys.* 79 (2011) 1030–1035.
- [20] K.H. Wu, T.H. Ting, C.I. Liu, C.C. Yang, J.S. His, Electromagnetic and microwave absorbing properties of Ni<sub>0.5</sub>Zn<sub>0.5</sub>Fe<sub>2</sub>O<sub>4</sub>/ bamboo charcoal core-shell nano-composites, *Compos. Sci. Technol.* 68 (2008) 132–139.